Partial 3D Shape Retrieval by Reeb Pattern Unfolding

Julien Tierny, Jean-Philippe Vandeborre, Mohamed Daoudi

Partial 3D Shape Retrieval by Reeb Pattern Unfolding

Julien Tierny[1], Jean-Philippe Vandeborre[1,2] and Mohamed Daoudi[1,2]

[1]LIFL (UMR USTL/CNRS 8022), Lille, France
[2]Institut TELECOM ; TELECOM Lille 1, France
{julien.tierny, jean-philippe.vandeborre, mohamed.daoudi}@lifl.fr

Abstract

This paper presents a novel approach for fast and efficient partial shape retrieval on a collection of 3D shapes. Each shape is represented by a Reeb graph associated with geometrical signatures. Partial similarity between two shapes is evaluated by computing a variant of their maximum common sub-graph.

By investigating Reeb graph theory, we take advantage of its intrinsic properties at two levels. First, we show that the segmentation of a shape by a Reeb graph provides charts with disk or annulus topology only. This topology control enables the computation of concise and efficient sub-part geometrical signatures based on parameterisation techniques. Secondly, we introduce the notion of Reeb pattern *on a Reeb graph along with its structural signature. We show this information discards Reeb graph structural distortion and still depicts the topology of the related sub-parts. The number of combinations to evaluate in the matching process is then dramatically reduced by only considering the combinations of topology equivalent Reeb patterns.*

*The proposed framework is invariant against rigid transformations and robust against non-rigid transformations and surface noise. It queries the collection in interactive time (from 4 to 30 seconds for the largest queries). It outperforms the competing methods of the SHREC 2007 contest in term of NDCG vector and provides, respectively, a gain of 14.1% and 40.9% on the approaches by Biasotti et al. [BMSF06] and Cornea et al. [CDS*05].*

As an application, we present an intelligent modelling-by-example system which enables a novice user to rapidly create new 3D shapes by composing shapes of a collection having similar sub-parts.

Keywords: 3D shape retrieval, reeb graph theory, partial matching, shape signature, modeling-by-example

ACM CCS: H.3.1 [Information Storage and Retrieval]: Content Analysis and Indexing I.3.5 [Computer graphics]: Computational Geometry and Object Modelling

1. Introduction

Three dimensional (3D) shape retrieval systems based on visual similarity aim at helping human users browsing large collections of 3D shapes in an interactive and intuitive way. In this framework, the user specifies a 3D model as an example query and the system is expected to sort the entries of the collection by decreasing visual similarity, providing as top results the most similar entries.

An important literature has been provided for shape retrieval based on global similarity, presenting methods en-

abling retrieval of similar objects despite rigid transformations [CTSO03, FMK*03] or even non-rigid transformations (such as shape bending or character articulation) [HSKK01]; [GSCO07]; [JZ07]. We defer the reader to survey articles [TV04, BKS*05, IJL*05] for a broad overview of retrieval methods based on global similarity.

However, other applicative contexts, such as modelling-by-example [FKS*04] (where new shapes are created by cutting and pasting existing shape sub-parts) or classification [HKDH04], might require to retrieve objects with regard to *partial* similarity. In such a paradigm, systems are expected

to retrieve objects that have *similar sub-parts* even if they visually differ globally.

Unlike shape retrieval based on global similarity, only few papers have addressed the partial shape retrieval problem, while it is seen as the next challenging open issue by the shape retrieval community [CTSO03, FMK*03]. Moreover, it is a more general problem than global shape similarity estimation (two globally similar shapes will also be similar partially) and thus it is a research topic of larger impact.

Partial shape retrieval state-of-the-art techniques can be roughly classified into two categories.

On the one hand, local descriptors-based techniques aim at characterizing the local properties of a large number of small features extracted on the shape. Then, partial shape similarity is estimated by feature point-to-point matching and matching similarity estimation. Liu *et al.* [LZQ06] propose to use a Monte-Carlo sampling on the surface model and to capture the local aspect of the shape with spin-image signatures [JH99]. Funkhouser and Shilane [FS06] present a more sophisticated sampling strategy and then describe local geometry with several descriptors based on Spherical Harmonics [FMK*03] but this method is only experimented for global shape retrieval. In order to deal with the combinatorial explosion due to individual local feature comparison, such approaches use complex data structures to drive the feature matching process, such as priority queues [FS06] or feature clusters [LZQ06] inspired by text-document analysis. Gal *et al.* [GCO06] present an interesting geometrical hashing mechanism associated with a local surface description based on curvature analysis. In the context of Euclidean partial self symmetry detection, Mitra *et al.* [MGP06] use a similar approach by sampling the surface and associating samples with geometrical signatures based on normal cycles [CSM03]. Then, the authors propose a sample pruning strategy specific to symmetry characterization. However, as underlined by Biasotti *et al.* [BMSF06], most of local descriptor methods base their partial similarity estimation on point-to-point matching only. This is particularly detrimental in term of re-usability in application contexts such as modelling-by-example [FKS*04], where the similar sub-parts have to be explicitly identified and extracted.

On the other hand, structural-based approaches present the advantage to explicitly identify the surface patches that have been matched. Moreover, the combinatorial explosion due to feature comparison can be easily reduced by reasoning on the structure of the shape instead of using complex hashing mechanisms. These methods first segment the shape and represent it by a graph (or a skeleton [DJ06]) depicting the structural relations between the segments. Then, partial shape similarity is estimated using graph matching techniques. Cornea *et al.* [CDS*05] propose to extract the curve-skeleton of the shape and then employ the Earth Mover's Distance [KSDD03] to evaluate the partial similarity of the skeletons. However, sub-part signature is based on the euclidean distance between the surface and its skeleton which makes the method quite sensitive to non-rigid transformations. Biasotti *et al.* [BMSF06] present an efficient method based on Reeb graphs and Spherical Harmonics [FMK*03]. However, even if the Reeb graph construction algorithm is robust to non-rigid transformations (such as shape bending or character articulation), sub-parts signatures (spherical harmonics) are not, which is slightly detrimental to the overall robustness of the approach.

In this paper, we present a fast and efficient structural-oriented approach for partial 3D shape retrieval, based on Reeb graphs—an expressive topological shape description which has already shown its utility in several computer graphics applications [BMS00, ZMT05, AHLD07] (see [BGSF08] for a recent survey). Unlike previous works based on Reeb graphs [HSKK01, TS05] and which have been specifically designed for global shape retrieval (using a multi-resolution strategy), this work presents a framework for *partial* similarity retrieval (retrieving objects that have similar sub-parts even if the visually differ globally). Moreover, in comparison with the technique proposed by Biasotti *et al.* [BMSF06], this paper introduces a novel description (which is pose insensitive) and a new partial comparison method. The main contribution of this work is to take advantage of the intrinsic properties of Reeb graph theory to improve both the shape description and comparison processes. First we segment the shape using a Reeb graph and encode the relations between resulting patches into a dual Reeb graph. We show this segmentation provides only two types of charts, called *Reeb charts*, that have either disk or annulus topology. This topology control enables efficient pose insensitive sub-part geometrical description based on parameterisation techniques [WWJ*06, TVD07]. Secondly, we introduce the notion of *Reeb pattern* on a Reeb graph along with its structural signatures. We show this information discards Reeb graph structural distortion and avoids the use of error-tolerant graph matching algorithms [MB98]. Moreover, *Reeb pattern* structural signatures concisely encode the related sub-part topology and enable to dramatically reduce the number of combinations to evaluate in the matching process by only considering the combinations of topology equivalent *Reeb patterns*.

After a brief method overview, we describe the Reeb graph segmentation process and detail the sub-part geometrical signature computation. Then, we introduce the notion of Reeb pattern and present the partial similarity estimation algorithm based on Reeb pattern unfolding (RPU). Finally, we show experimental results that demonstrate the performance improvement and the robustness of our method. We also describe an intelligent modelling-by-example system that demonstrates the applicative interest of our framework.

2. Method Overview

Let M be a closed 2-manifold of arbitrary genus embedded in $\mathbb{R}^3$. First, we compute the Reeb graph of M to segment it into a set of charts C_i of controlled topology, which we call *Reeb charts*, which have either disk or annulus topology. Then, for each chart, we compute its unfolding signature λ_{ϕ_i} (as introduced in [TVD07]) by measuring the distortion of its mapping ϕ_i to the canonical planar domain D (either the unit disk or the unit annulus). Finally, the input manifold is represented by a dual Reeb graph noted $\mathcal{R}$ associated with the unfolding signatures of the Reeb charts.

To measure the partial similarity between two dual Reeb graphs $\mathcal{R}_1$ and $\mathcal{R}_2$, approximations of their maximally similar common sub-graphs $\mathcal{G}_1^*$ and $\mathcal{G}_2^*$ are computed. In particular, to reduce the number of combinations to consider, we use the following strategy. First, the sets $\mathcal{P}_1$ and $\mathcal{P}_2$ of topology equivalent *Reeb patterns* belonging, respectively, to $\mathcal{R}_1$ and $\mathcal{R}_2$ are detected. Then, the set $\mathcal{M}$ of all possible mappings m between topology equivalent *Reeb patterns* of $\mathcal{P}_1$ and $\mathcal{P}_2$(m : $\mathcal{P}_1 \rightarrow \mathcal{P}_2$) is computed. In practice, the average cardinality of $\mathcal{M}$ is 20. For each mapping m, an expansion algorithm simultaneously expands the common sub-graphs $\mathcal{G}_1^m$ and $\mathcal{G}_2^m$ in $\mathcal{R}_1$ and $\mathcal{R}_2$.

Each mapping m is scored relatively to the geometrical similarity $S(m)$ between the two common sub-graphs $\mathcal{G}_1^m$ and $\mathcal{G}_2^m$. $S(m)$ is computed by comparing the unfolding signatures λ_{ϕ_i} and λ_{ϕ_j} of the pairs of matched Reeb charts C_i and C_j. Let $\widehat{m^*}$ maximize on $\mathcal{M}$ the similarity S between its related sub-graphs $\widehat{\mathcal{G}_1^*}$ and $\widehat{\mathcal{G}_2^*}$. The similar sub-parts of two closed 2-manifolds M_1 and M_2 are identified by $\widehat{\mathcal{G}_1^*}$ and $\widehat{\mathcal{G}_2^*}$. Moreover, the partial similarity between M_1 and M_2 is given by $S(\widehat{m^*})$. Algorithm 1 summarizes the overall process.

Algorithm 1 Partial shape retrieval algorithm overview.

Compute the query shape's Reeb graph $\mathcal{R}_q$
for all $C_i \in \mathcal{R}_q$ **do**
    Compute C_i unfolding signature.
end For
Compute $\mathcal{R}_q$ structural signatures.
for all $\mathcal{R}_c$ in the collection index **do**
    Compute the set $\mathcal{M}$ of mappings m between
    topology equivalent Reeb patterns of $\mathcal{R}_q$ and $\mathcal{R}_c$.
    for all $m \in \mathcal{M}$ **do**
        Expand recursively m to patterns' neighbour charts.
        Evaluate $S(m)$.
    end for
    Return $S(\widehat{m^*})$ as the partial
    similarity between $\mathcal{R}_q$ and $\mathcal{R}_c$
end for
Sort the collection entries according to their partial
    similarity to the query shape.

---

3. Reeb Graph and Unfolding Signatures

Given an input closed 2-manifold M of arbitrary genus, the first step of the framework, the shape description step, consists in segmenting M using its Reeb graph [Ree46] and to compute a geometrical signature for each extracted surface segment.

3.1. Reeb graph segmentation

Definition 1 (Reeb graph) Let $f : M \rightarrow \mathbb{R}$ be a simple Morse function defined on a compact manifold M. The Reeb graph $R(f)$ is the quotient space on $M \times \mathbb{R}$ by the equivalence relation $(p_1, f(p_1)) \sim (p_2, f(p_2))$, which holds if $f(p_1) = f(p_2)$ and p_1, p_2 belong to the same connected component of $f^{-1}(f(p_1))$.

To deal with invariance to rigid transformations and robustness to non-rigid ones, we compute the Reeb graph of the input 2-manifold (represented by a triangulation noted T) using a function based on geodesic distances. In particular, to introduce some *visual semantics* in the segmentation, we automatically extract feature points (vertices located on the extremity of prominent components, see implementation details in Section 3.3). For each vertex $v \in T$, $f(v) = \delta(v, v_f)$ where δ stands for the geodesic distance and v_f for the closest feature point from v. Figure 2(a) shows the level lines of f and the feature points of T (in green). This computation of the f function has been preferred to the integral geodesic approximation [HSKK01] or a harmonic function [NGH04] because it gives better emphasis on local shape features (like fingers or ears) thanks to the feature points, which is crucial for partial matching.

Definition 2 (Reeb chart) Let $\Psi \colon M \rightarrow R(f)$ map each point p of M to its equivalence class in $R(f)$. Let $E = \{E_0, \ldots E_n\}$ be the edges (maximally connected unions of equivalence classes containing only regular points of f) of the Reeb graph $R(f)$. $C_i = \Psi^{-1}(E_i)$ is defined as a *Reeb chart*.
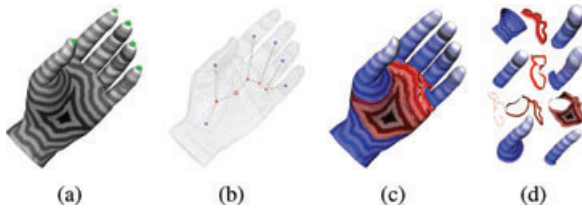
Figure 2(b) shows a dual Reeb graph (where each edge E_i is collapsed in a coloured node and where black arcs represent adjacency relations between edges). Figure 1 gives more example of feature points, f functions and dual Reeb graphs. Figure 2(c) and 2(d) show the segmentation of the hand model into its Reeb charts. Basically, Reeb charts are the surface patches that correspond to the nodes of the dual Reeb graph.

Statement 1 (Reeb chart topology) Reeb charts of a compact closed orientable 2-manifold have either disk or annulus topology whatever the genus of the manifold is.

This statement can be briefly argued as follows. By definition, an edge E_i has two extremities, whose pre-images by Ψ are circles which form the two boundary components of the closure of the chart C_i. Hence, the closure of the Reeb charts has two boundary components. Morever, C_i has genus

Figure 1: *Feature points and f functions (first row) and dual Reeb graphs (second row) of several surface models.*

Figure 2: *Segmentation of a hand surface model into its Reeb charts.*

Figure 3: *Disk-like chart unfolding signature computation.*

zero. Thus Reeb charts have the topology of an open annulus (by definition, critical points and, particularly, saddle points equivalence classes are not included in Reeb charts).
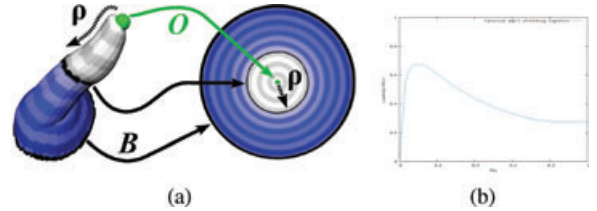
Disk-like Reeb charts constitute a specific case. We call a disk-like Reeb chart a Reeb chart which is adjacent to only one local extremum of f. As the related boundary component collapses to a point (the extremum), that kind of chart is given the topology of an open disk.

In Figure 2(d), disk-like Reeb charts have been coloured in blue and annulus-like ones in red. Notice that this decomposition brings a certain *visual semantic*: each of the fingers of the hand model forms a distinct chart.

3.2. Reeb chart unfolding signatures

To achieve efficient pose-insensitive geometrical signature computation for each Reeb chart C_i, we propose to characterize C_i by parameterisation techniques [WWJ*06, TVD07], especially by its mapping ϕ_i to the canonical planar domain D. In particular, we propose to compute C_i unfolding signature [TVD07], a concise vector that describes the evolution of the area distortion introduced by a planar mapping, as summarized below. Thanks to the Reeb graph properties, only two cases had to be considered: disk-like charts and annulus-like charts (cf. statement 1).

Given a disk-like chart C_i, let O be the local extremum of f it contains and B its boundary. We let ϕ_i map O to the centre of the unit planar disk, B to its boundary and f level lines to concentric circles, as shown in Figure 3, where the

thumb of the hand of Figure 2 has been mapped to the planar domain D.

Let $\rho(p) \in]0, 1[$ be the normalized absolute difference of f values between O and a point $p \in C_i$, as shown in Figure 3. Consequently to the Reeb chart definition, the sub-level set of ρ ($\{(p_1, p_2 \ldots p_n)|\rho(p_1, p_2, \ldots p_n) < \rho_0\}$) have also disk topology, as illustrated by the white sub-level set in Figure 3. As ρ increases, the shape of the ρ sub-level sets varies. Thus it induces an evolution in the distortion introduced by their mapping to D. Consequently, to capture the evolution of the sub-level set shape variation, the unfolding signature λ_{ϕ_i} of ϕ_i is defined as follows:
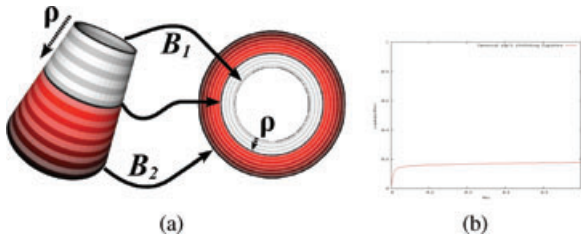
$$\lambda_{\phi_i}(\rho) = \frac{A_{C_i}(\rho)}{A_D(\rho)} = \frac{A_{C_i}(\rho)}{\pi \rho^2}, \qquad (1)$$

where $A_{C_i}(\rho)$ stands for the area of the sub-level set for parameter ρ on the original surface (C_i) and $A_D(\rho)$ stands for the area of the sub-level set on D. $A_{C_i}(\rho)$ is computed by summing the areas of the related triangles of T (after having normalized edge length by f, similarly to ρ).

Roughly, $\lambda_{\phi_i}(\rho)$ depicts the *stretch* one has to apply on the chart to map it to a disk as ρ increases.

As shown in [TVD07], as f is based on geodesic distances, the parameterisation (and thus its signatures) is invariant to rigid transformations and robust to non-rigid transformations. Moreover, it is also robust to surface noise.

An analog reasoning can be applied for annulus-like charts. Let B_1 be the boundary of shortest perimeter of an annulus-like chart C_j and B_2 the other one. In this case, we let ϕ_j

Figure 4: *Annulus-like chart unfolding signature.*

map B_1 to the inner boundary of the unit planar annulus and B_2 to its outer boundary, as shown in Figure 4. By defining the ρ parameter similarly to the previous case, the signature λ_{ϕ_j} of ϕ_j is computed as follows (1 is the inner radius of the unit annulus):

$$\lambda_{\phi_j}(\rho) = \frac{A_{C_j}(\rho)}{A_D(\rho)} = \frac{A_{C_j}(\rho)}{\pi(\rho+1)^2 - \pi}. \qquad (2)$$

3.3. Implementation details

For feature point extraction, among existing techniques [KLT05, LZ07, TVD08], we used the approach described in [TVD08] as at least two antipodal feature points are always guaranteed to be extracted (so f can always be computed). This technique proposes to identify the extremities of prominent components by intersecting the sets of extrema of two scalar functions based on the geodesic distances to two automatically extracted antipodal vertices [TVD08]. It runs in $O(n \log(n))$ steps with n being the number of vertices in the surface mesh and the extraction is robust to noise and invariant to isometric transformations.

Regarding the Reeb graph computation, the geodesic distance to feature points function does not necessarily fulfill all the requirements of a simple Morse function: (i) smoothness, (ii) distinctly valued critical points and (iii) non-degenerate critical points. Thus, we propose a strategy based on f perturbation to guarantee Reeb graph intrinsic properties (especially about the degree of its nodes). First, (i) f is not differentiable in the configurations of the surface where points are geodesic-equidistant from several feature points. In the discrete setting, this phenomenon leads to the apparition of additional maxima and saddles in these configurations. To cancel these specific critical points, we propose a strategy based on global perturbation, used in [TVD08] on a similar function in the context of skeleton extraction. Starting from the feature points (f minima in this paper), the algorithm iteratively visits the surface mesh by propagation, using a variant of Dijkstra's algorithm (which uses f as weight). Let v be the vertex visited at a given step of such a sweep, the set of vertices candidate for visit (plus the edges linking them) form an upper-value approximation of $f^{-1}(f(v))$ (level line approxi-

mation). Then topological variations are encoded in the graph at iterations where connected components of the level line approximation (*contour* approximations) split or merge (see [TVD08] for further details). As the algorithm visits one vertex per iteration, this process is equivalent to considering for each vertex its visit iteration number as f value. This perturbation simulates value uniqueness (ii). Moreover, as additional critical points located in areas where f is non-differentiable are visited iteratively, they are attributed distinctly increasing values, cancelling pairs of extra maxima and saddles (i). Additionally, if a contour approximation splits in $k+1$ sets from an iteration to another with $k \geq 2$ (or if $k+1$ contour approximations merge into one), a multiple k-saddle unfolding strategy [EHZ01] is used to simulate k simple saddles. This technique transforms degenerate critical points into non-degenerate ones (iii) [EHZ01, CMEH*03].

At this stage of the framework, the input closed 2-manifold M is concisely represented by a dual Reeb graph $\mathcal{R}$, whose nodes are accompanied with the unfolding signatures of corresponding Reeb charts. In particular, each unfolding signature is stored as a vector of real values (using a pre-defined number of samples, 64 in all of our experiments).
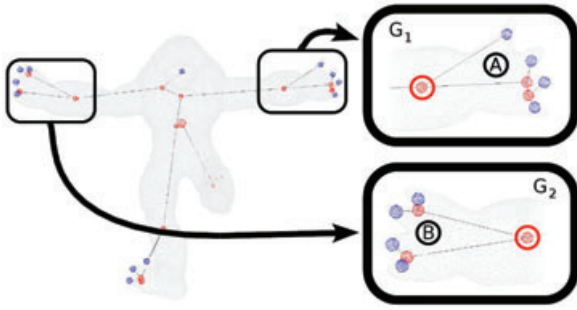
4. Reeb Pattern-based matching algorithm

The next step of the framework consists in shape partial similarity estimation. Given two input 2-manifolds M_1 and M_2, the goal is to identify their similar sub-parts and to evaluate their geometrical similarity.

4.1. Problem statement

Given two dual Reeb graphs $\mathcal{R}_1$ and $\mathcal{R}_2$, the goal would be to find an optimal injective mapping m^* between a sub-graph $\mathcal{G}_1^* \in \mathcal{R}_1$ and a sub-graph $\mathcal{G}_2^* \in \mathcal{R}_2$ which maximizes a similarity function $S(m^*)$, computed relatively to the geometrical signatures of the nodes matched by m^*.

A brute-force approach to this problem consists in computing the set $\mathcal{M}$ of all the possible injective mappings $m : \mathcal{R}_1 \to \mathcal{R}_2$, then identifying through an expansion process the common sub-graphs $\mathcal{G}_1^m \in \mathcal{R}_1$ and $\mathcal{G}_2^m \in \mathcal{R}_2$ (such that $m : \mathcal{G}_1^m \to \mathcal{G}_2^m$ is an isomorphism) and finally evaluating their geometrical similarity $S(m)$. The solution of the problem would be the mapping $m^* \in \mathcal{M}$ that would maximize S. Let n and k be, respectively, the number of nodes of the largest and the smallest of the two dual Reeb graphs to compare. With such an approach, $|\mathcal{M}| = \frac{n!}{(n-k)!}$, which results in an exponential time complexity evaluation process. Moreover, in practice, as underlined by Messmer and Bunke [MB98], graphs representing real world objects may be affected by noise or distortion, motivating the use of error-tolerant matching algorithm, whose complexity is generally even greater than exact algorithms [MB98].

Figure 5: *Structural distortion on two visually similar and topology equivalent Reeb patterns.*

Figure 6: *Structural signatures of a genus-0 and a genus-1 Reeb pattern.*

In the following paragraphs, we describe Reeb graph structural distortion and propose a structural signature for Reeb patterns insensitive to such a distortion (avoiding the need for error-tolerant matching algorithm). Finally, for partial similarity estimation, we dramatically reduce the search space of the problem by considering the set of all the possible injective mappings between topology equivalent Reeb patterns only.
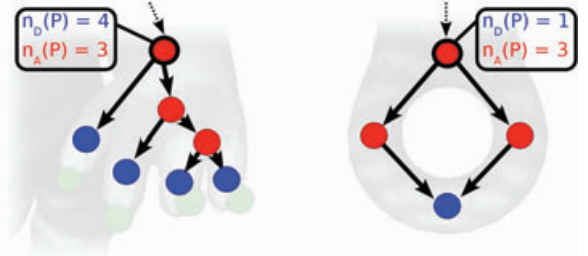
4.2. Reeb pattern and structural distortion

Definition 3 (Reeb pattern) Let M be a compact closed 2-manifold embedded in $\mathbb{R}^3$, $R(f)$ its Reeb graph and C_i an annulus-like Reeb chart. Let B^+ be the boundary component of C_i with highest f value, noted f_{B^+}. Let M^- be the sub-level set of M associated to the f_{B^+} value ($M^- = \{p \in M \,|\, f(p) < f_{B^+}\}$). The *Reeb pattern* P_i associated to the annulus-like Reeb chart C_i is the connected component of M^- having B^+ as only boundary component.

Figure 5 shows an Armadillo with its dual Reeb graph and zooms in two Reeb patterns P_1 and P_2 and their related sub-graphs G_1 and G_2. Moreover, the annulus-like charts associated to P_1 and P_2 have been marked with a red circle. Roughly speaking, a Reeb pattern P_i is a surface sub-part which includes nearby protrusions (this is a set of annulus and disk-like charts, delimited by C_i boundary). Notice Reeb patterns are not necessarily defined for each annulus-like Reeb chart (they are not defined for pairs of charts forming handles).

Dual Reeb graphs can suffer from noise and distortion. From our experiences, feature point extraction is very stable on similar objects. This means very few noise due to inexact feature point extraction will appear. However, dual Reeb graphs still suffer from distortion.

Morse theory [Mil63] states that any smooth function on a manifold can be transformed into a Morse function by a slight perturbation, which transforms degenerate critical points into non-degenerate ones. This result depicts the fact that small perturbations on the function can drastically change the properties of the critical points. In particular, in our case, a slight perturbation on the surface (and thus on the function) can change the sequence of bifurcations and junctions in the corresponding dual Reeb graph. As a consequence, in Figure 5, the sub-graph G_1 first bifurcates in the A-labelled region while the sub-graph G_2 first bifurcates in the B-labelled region. Consequently, no isomorphism exists between G_1 and G_2 while the two related Reeb patterns (the hands of the Armadillo) are visually similar and topology equivalent. We refer to this phenomenon as Reeb graph *structural distortion*.

To overcome this issue, in order to compare topology equivalent Reeb patterns despite structural distortion, we introduce the notion of *structural signature* of a Reeb pattern.

Definition 4 (Reeb pattern structural signature) Let M be a compact closed 2-manifold embedded in $\mathbb{R}^3$ and P_i a Reeb pattern associated to an annulus-like Reeb chart C_i. Let $n_D(P_i)$ and $n_A(P_i)$ be, respectively, the number of disk-like and annulus-like Reeb charts included in P_i. The couple $(n_D(P_i), n_A(P_i))$ is the structural signature of P_i.
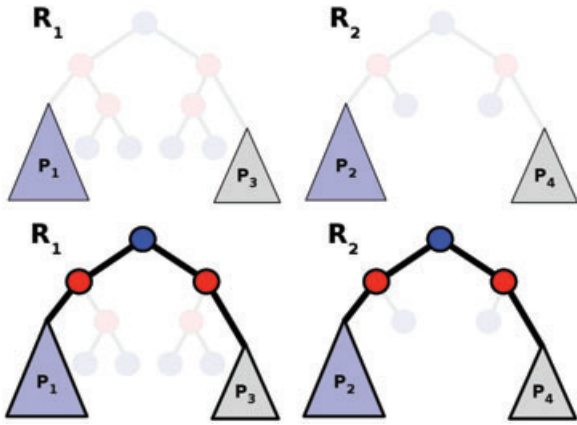
Statement 2 (Structural signature topological properties) The structural signature of P_i describes P_i topology since $n_D(P_i)$ and $n_A(P_i)$ are linked by the following relation:

$$n_D(P_i) = n_A(P_i) + 1 - 3g_{P_i} \qquad (3)$$

with g_{P_i} the genus of the Reeb pattern.

A proof of Equation (3) is given in Appendix A. By definition, all Reeb patterns are 2-manifolds with one boundary. In term of topology description, only their genus differs. Thus their topology is fully described through their structural signature. Moreover, this signature does not encode the way the bifurcations and junctions are sequenced in the Reeb pattern. Thus it does not depict structural distortion.

Figure 6 gives two examples of structural signatures of a genus-0 and a genus-1 Reeb pattern. In the rest of the approach, structural signatures help us both overcoming structural distortion and reducing the search space of the problem.

Figure 7: *Expansion example: for a given combination of topology equivalent Reeb patterns ((P_1, P_2) and (P_3, P_4)), the expansion algorithm tries to expand as much as possible the common sub-graphs (in bold in the second row).*

Figure 8: *Expansion process from two topolgy equivalent Reeb patterns P_1 and P_2. Steps **1**, **2** and **3** are depicted by blue arrows.*

4.3. Maximally similar common sub-graph approximation

In the following paragraphs, we introduce an efficient approximation of the brute-force approach that does not consider all the node-to-node combinations but the topology equivalent Reeb pattern to topology equivalent Reeb pattern combinations only.

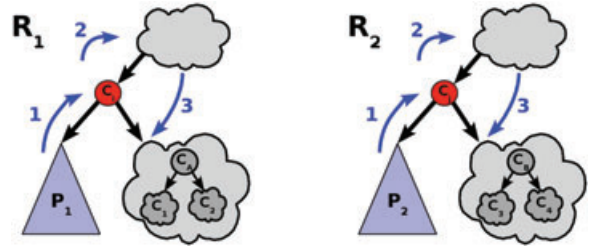#### 4.3.1. *Reeb pattern combination enumeration*

First, the structural signature of each Reeb pattern P_i of each of the two dual Reeb graph $\mathcal{R}_1$ and $\mathcal{R}_2$ is computed.

Then, for each identified Reeb pattern P_i, we compute the set of topology equivalent Reeb patterns (whose structural signatures are identical) in the other graph. Let $\mathcal{P}_1$ and $\mathcal{P}_2$ be respectively the sets of Reeb patterns of $\mathcal{R}_1$ and $\mathcal{R}_2$ that have a *homologue* in the other graph (whose structural signatures are identical).

Next, we compute the set $\mathcal{M}$ of all the possible injective applications $m : \mathcal{P}_1 \to \mathcal{P}_2$ that map a Reeb pattern $P_1 \in \mathcal{P}_1$ to a homologue Reeb pattern $P_2 \in \mathcal{P}_2$. In our experiments, the average cardinality of $\mathcal{M}$ is 20 (which has no comparison with the $\frac{n!}{(n-k)!}$ combinations of the brute-force approach).

4.3.2. *Expansion of common sub-graphs*

Next, the common sub-graphs $\mathcal{G}_1^m \in \mathcal{R}_1$ and $\mathcal{G}_2^m \in \mathcal{R}_2$ are built for each m thanks to an expansion algorithm that simultaneously visits $\mathcal{R}_1$ and $\mathcal{R}_2$, starting by Reeb pattern associations. As illustrated in the example of Figure 7, this

algorithm expands the initial mapping m by recursively visiting the nodes adjacent to associated Reeb patterns.

Step 1 Considering $\mathcal{R}_1$ and $\mathcal{R}_2$ as directed acyclic graphs (the direction goes towards decreasing f values), the algorithm first visits the *parent nodes* C_i and C_j of P_1 and P_2, as shown in Figure 8 (step **1**). If the degree or the type of C_i and C_j differs, the expansion stops at this point and restarts from another unvisited pair of topology equivalent Reeb patterns. Otherwise, the expansion continues. In the case of orientable 2-manifolds, the degree of an equivalence class of a saddle point in the Reeb graph always equals 3 [Ree46]. As a consequence, two more steps, at most, have to be considered (labelled **2** and **3** in Figure 8).

Step 2 The step **2** recursively repeats steps **1**, **2** and **3** in this order. This means the expansion continues the same way as far as visited nodes have the same degree. Moreover, it stops when nodes corresponding to Reeb patterns explicitly matched by m are reached.
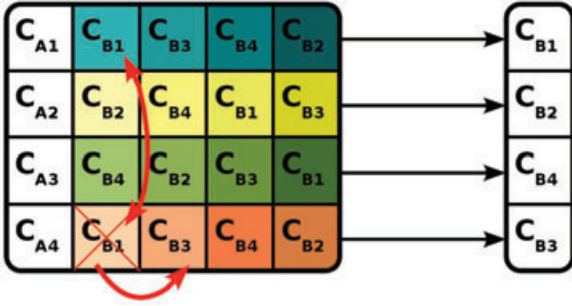
Step 3 In step **3**, the expansion continues with the same stopping condition. However, let C_A and C_B be two nodes that have been matched in step **3**. If their degree equals 3, a decision has to be taken as for the matching of their *children* C_1, C_2 and C_3, C_4 (see Figure 8). *Children* whose Reeb patterns are explicitly matched by m are by definition associated. Remaining nodes are matched according to their degree and their structural signature. At this point, if no decision can be taken according to this criterion, the expansion stops and restarts from another unvisited pair of homologue Reeb patterns.

The output of this algorithm are two common sub-graphs $\mathcal{G}_1^m$ and $\mathcal{G}_2^m$, along with their node and Reeb pattern matches.

4.3.3. *Intra-Reeb pattern node-to-node matching*

The previous algorithm outputs node and Reeb pattern associations. In order to have a full node-to-node correspondence between the two sub-graphs to compare, we have to find a

Figure 9: *Intra-Reeb pattern node-to-node matching (bipartite matching approximation).*

Figure 10: *Reeb chart (bright colors) and pattern (dark colors) matching between a boy and a centaur. Unmatched charts are black. Even though the hands do not have the same number of fingers (some are stuck together on the left model and count for one), they still have been matched.*

node-to-node mapping for each pair of topology equivalent Reeb patterns matched by m (like P_1 and P_2 in Figure 8). Due to possible structural distortion, there might be no isomorphism between the sub-graphs G_1 and G_2 of P_1 and P_2.

Consequently, intra-Reeb pattern node matching is driven by geometrical similarity only running a bipartite matching algorithm, which tries to match the most similar nodes while maximizing the sum of similarities on the patterns. In practice, we run a polynomial approximation of this algorithm as shown in Figure 9. Let $\mathcal{C}_A$ and $\mathcal{C}_B$ be, respectively, the set of disk charts of P_1 and P_2. For each chart $C_{A_i} \in \mathcal{C}_A$, the charts of $\mathcal{C}_B$ are sorted by decreasing values of the geometrical similarity function $s \in [0, 1]$, as shown in the example of Figure 9:

$$s(C_{A_i}, C_{B_j}) = 1 - L_{N1}(C_{A_i}, C_{B_j}), \tag{4}$$

where L_{N1} is the normalized L_1 distance between the unfolding signatures of C_{A_i} and C_{B_j}. Then, the pair of most similar charts are matched. If conflicts occur (see C_{B_1} in the example of Figure 9), only the best matches ((C_{A_1}, C_{B_1}) in the example) are kept unchanged until no more conflict persists. By definition of the Reeb pattern structural signature $|\mathcal{C}_A| = |\mathcal{C}_B|$, thus this algorithm is guaranteed to converge to a solution. Finally, the same process is achieved for the annulus-like charts of P_1 and P_2. At this stage of the algorithm, m is a full node-to-node correspondence between $\mathcal{G}_1^m$ and $\mathcal{G}_2^m$.

4.3.4. *Similarity estimation*

In this step of the comparison, each mapping m is scored relatively to the geometrical similarity S of associated common sub-graphs $\mathcal{G}_1^m$ and $\mathcal{G}_2^m$. At this point, several similarity functions can be defined. In our experiments, we use the following function:

$$S(m) = \frac{\sum_{\forall C_i \in \mathcal{G}_1^m}(1 - L_{N1}(C_i, m(C_i)))^\alpha}{|\mathcal{R}_q|}. \tag{5}$$

In Equation (5), $L_{N1}(C_i, m(C_i))$ stands for the normalized L_1 distance between the unfolding signatures of C_i and $m(C_i)$. α stands for a corrective parameter whose aim is to amplify the geometrical similarity contribution (after training, α is set to 4). Finally $|\mathcal{R}_q|$ stands for the number of nodes of the dual Reeb graph that represents the query model presented to the system. Notice this similarity measure does not respect symmetry or triangular inequality (an object can share similar parts with two other objects that are not similar).
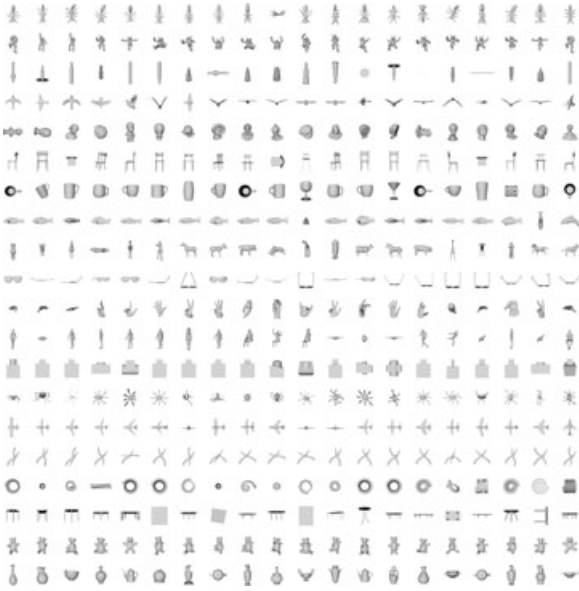
Finally, the mapping $\widehat{m^*}$ that maximizes S is the approximation of the optimal solution m^*. Moreover, $\widehat{\mathcal{G}_1^*}$ and $\widehat{\mathcal{G}_2^*}$ are the approximations of the most similar sub-parts of two 2-manifolds M_1 and M_2, whose partial similarity is given by $S(\widehat{m^*})$. Figure 10 shows an example of the approximated optimal mapping $\widehat{m^*}$ between two sub-graphs $\widehat{\mathcal{G}_1^*}$ and $\widehat{\mathcal{G}_2^*}$ of two surface models, along with the node-to-node and pattern-to-pattern matching.

5. Experiments and Results

To assess the efficiency of the framework, we evaluate its performance on the SHape Retrieval Contest (SHREC) 2007 partial retrieval benchmark [MPB07], and make some comparisons with the methods competing to this contest.

5.1. Partial retrieval benchmark description

This benchmark is composed of a data-set of 400 manifold models (grouped in 20 classes, see Figure 11) and of a query-set of 30 manifold models (see Figure 12). The data-set exhibits diverse variations, from pose change, to shape variability within a same class or topology variation (notice 4 of the 20 classes contain non-zero genus surfaces). Each query shares visually similar sub-parts with at least two classes of the data-set. Figures 13, 14 and 15 show three examples of typical queries and the models of the data-set retrieved by our system. Moreover, for a given query, the ground-truth divides the data-set into *Highly Relevant*, *Marginally Relevant*

Figure 11: *SHREC 2007 data-set snapshot (one class per row: ants, armadillos, bearings, birds, bustes, chairs, cups, fishes, four-legs, glasses, hands, humans, mechanics, octopuses, planes, pliers, springs, tables, teddies and vases).*

Figure 12: *SHREC 2007 query-set snapshot.*

and *Non-Relevant* class groups. This granularity enables to precisely evaluate the relevance of the results returned by the system. In particular, each relevance group is associated to a specific score, used in the computation of the Normalized Discounted Cumulated Gain (NDCG) vector. Roughly speaking, the higher is the NDCG[i] value, the more relevant are the top-i results. Such a performance measure provides a relevance overview over the whole the data-set. Moreover, it can take into account several classes for scoring a query, which is important for partial similarity since a query can be partially similar to several classes of objects. Furthermore, it is the only performance measurement taken into account in the contest (for more details, we defer the reader to the contest proceedings [MPB07]).

5.2. Experimental setup

The 400 models of the data-set are first indexed off-line. During the off-line process, the dual Reeb graph and the related unfolding signatures (using 64 samples) are computed for each model and stored into the index file of the data-set.

During the on-line process, the dual Reeb graph and the unfolding signatures of the query are first extracted. Then, its dual Reeb graph is compared with each graph of the index as described previously. Finally, the entries of the data-set are sorted by decreasing values of partial similarity. Depending on the number of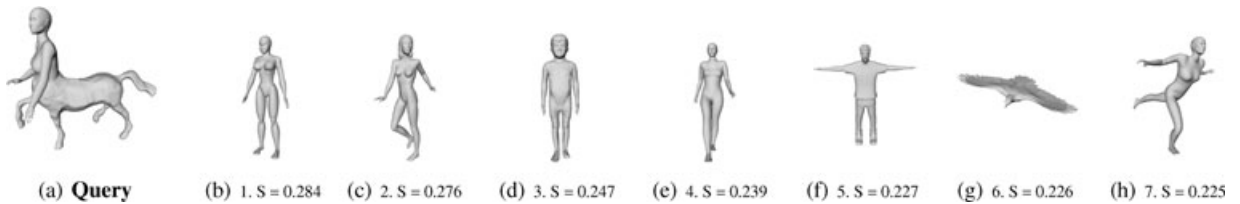 vertices in the query surface mesh and the size of the dual Reeb graph, the full processing time of a query varies from *4 to 30 seconds* on a 3GHz P4 PC.
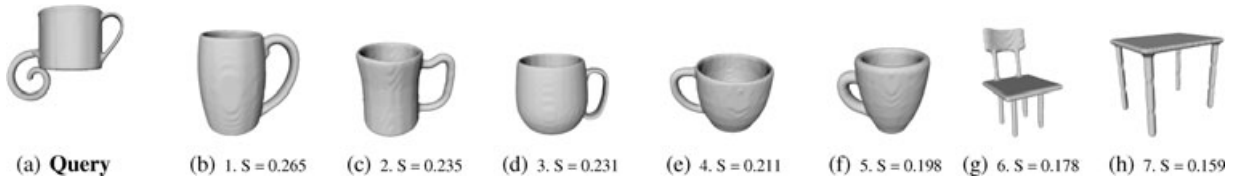
5.3. Framework performance evaluation

First, from a qualitative point of view, Figures 13, 14 and 15 give a good overview of the efficiency of the framework. For example, in Figure 13, the query is a centaur (half-horse, half-human) and thus most of the top-results are humanoid models (first horses are retrieved at rank 15), even if they are not globally similar to the query. Figure 14 demonstrates the method's ability to handle non-zero genus surfaces (the case of the two outliers, rank 6 and 7, is discussed in the limitation dedicated Section 5.5).

From a more quantitative point of view, in the first experiment, we compare the average NDCG vector of our approach with those of the methods competing the contest [CDS*05, BMSF06] (as reported in the contest proceedings [MPB07]). Such a vector is the average of the 30 NDCG vectors corresponding to the 30 models of the query-set. Figure 16 shows the curves corresponding to these vectors. As the RPU curve is higher than the others, it is obvious that it outperforms related methods. Moreover, to quantify its improvement, we introduce the NDCG vector gain G, which is the ratio of the area between two curves and the area below the lowest one:
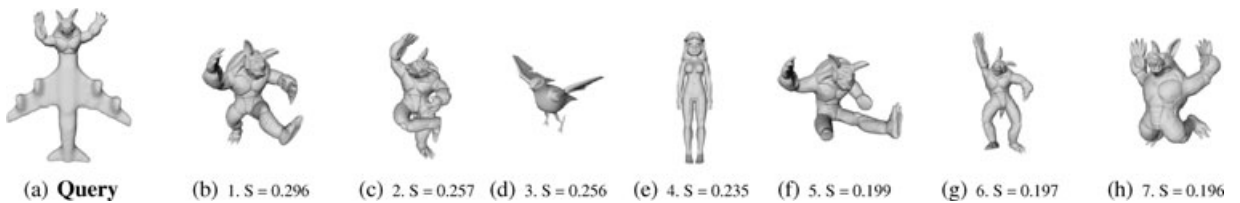
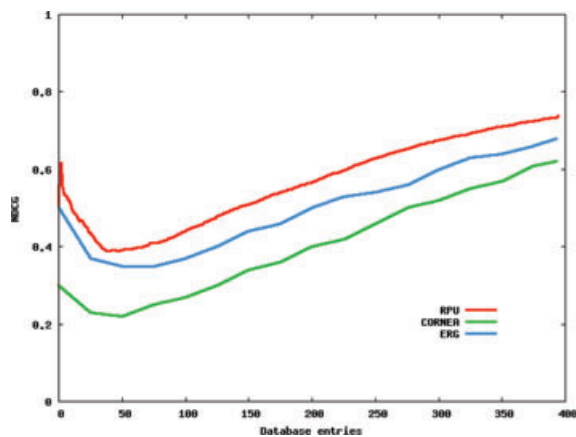$$G(A, B) = \frac{\sum_{i=1}^{400}(NDCG[i]_A - NDCG[i]_B)}{\sum_{i=1}^{400} NDCG[i]_B}. \quad (6)$$

Figure 13: *A query from the SHREC 2007 query-set (a centaur) and the top-7 results retrieved by the system.*

Figure 14: *A genus-1 query from the SHREC 2007 query-set and the top-7 results retrieved by the system.*

Figure 15: *Another query from the SHREC 2007 query-set (an Armadillo composed with a plane) and the top-7 results retrieved by the system. Notice that Armadillos have been retrieved despite their different poses.*

Figure 16: *Average normalized discounted cumulated gain (NDCG) vectors for Reeb pattern unfolding (RPU), Extended Reeb Graphs (ERG) and curve-skeleton based many-to-many matching (CORNEA) on the SHREC 2007 data-set.*

With such a measure, the gain on the methods by Biasotti *et al.* [BMSF06] and Cornea *et al.* [CDS∗05] is, respectively, of *14.1%* and *40.9%*. In the second experiment, we evaluate the impact of the choice of the similarity function S

(see Section 4.3.4) on the retrieval performances. In particular, we consider the function S_1 that returns the size of the common sub-graphs (the maximally similar common sub-graphs become then the maximum common sub-graphs). We also consider the function S_2 where the unfolding signatures have been replaced by the geometrical attributes used by Hilaga *et al.* [HSKK01]. The related curves are reported in Figure 17. This figure shows that performances comparable to the other methods are obtained with S_2. Moreover, it clearly demonstrates the gain provided by unfolding signatures.

5.4. Robustness evaluation

As the dual Reeb graph construction and the unfolding signature computation are based on normalized geodesic distance evaluation, the approach is guaranteed to be invariant against rigid-transformations. Moreover, Figure 15 demonstrates its robustness against non-rigid transformations, since Armadillos in different poses have been retrieved as top results. In the third experiment, we investigate the framework robustness against surface noise. In particular, for each element of the query-set, we added a surface noise whose amplitude is bounded by, respectively, $\pm 0.5\%$ and $\pm 1\%$ of the lengths of the bounding box of the model, as shown in Figure 18. The
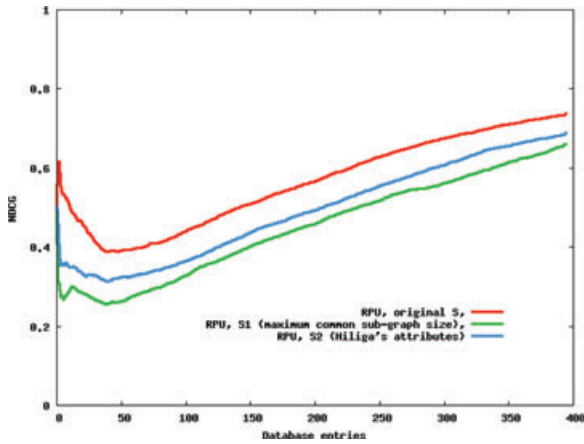
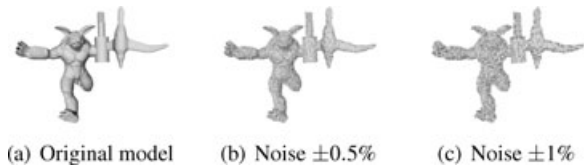**Figure 17:** *Contribution of the chart unfolding signatures to the performances.*

(a) Original model   (b) Noise ±0.5%   (c) Noise ±1%

Figure 18: *Surface noise on a SHREC 2007 query.*
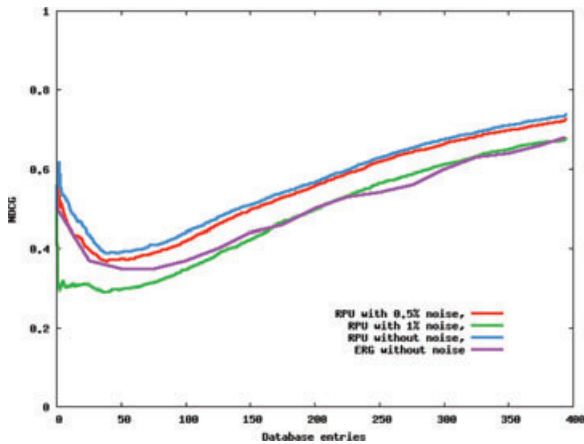

Figure 19: *Robustness evaluation of RPU with a noisy version of the SHREC 2007 query-set. Even with a surface noise of ± 0.5%, RPU still outperforms state-of-the-art techniques scores on clean data.*

NDCG vectors with such corrupted query-sets have been reported in Figure 19. These curves demonstrate the stability of the algorithm despite the noise. Moreover, even with a surface noise of ± 0.5%, it stills outperforms ERG [BMSF06] scores on clean data.
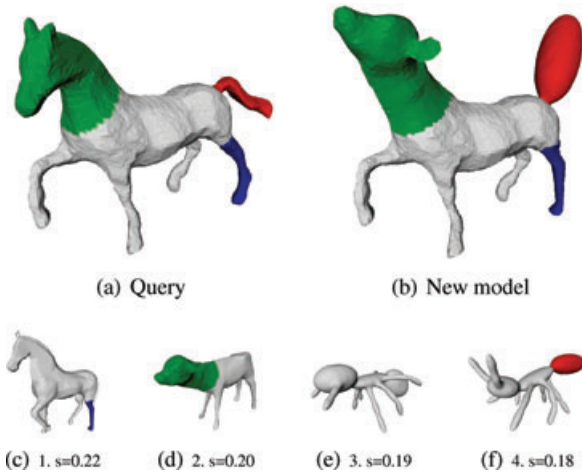
5.5. Discussion and limitations

As other structural based approaches, the surface decomposition step of the framework introduces a bias in the comparison process. To guarantee stability and performance, this decomposition has to be stable within a same class of objects and moreover coherent with the data-set ground-truth. The bias introduced in the presented technique is based on feature point extraction (which drives the surface segmentation). Hence, this stage is a critical part of the framework and impacts its performances. In practice, with the SHREC data-set, feature extraction turns out to be homogeneous within most classes. As a counter-example, the *four legs* class is composed of models representing distinct types of animals, having different protrusions (with or without tail, horns, etc.) and thus leads to slightly distinct decompositions. In the future, we would like to investigate other decomposition strategies that would overcome this issue but still take into account local shape features.
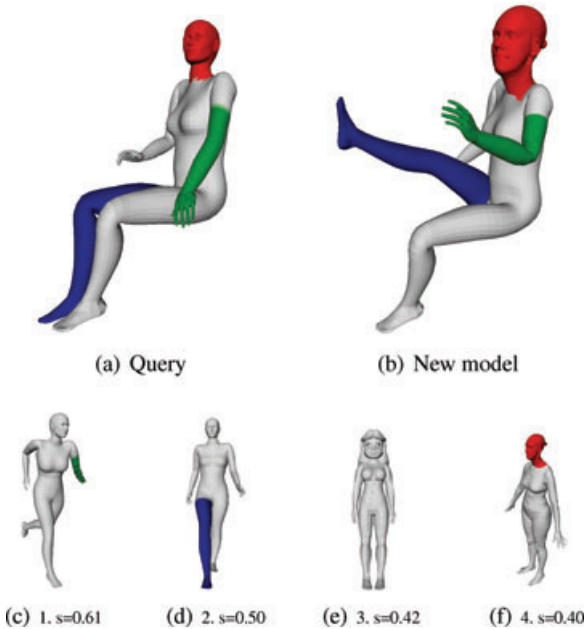
Moreover, as the decomposition and matching processes are topology based, the overall framework is quite sensible to topology variations within a same class of objects. For example, most of humanoids are modelled with genus zero surfaces but if a humanoid's feet are stuck to each other the related surface will have genus one and consequently the legs will mainly match with objects having handles. Same remarks go to the example of Figure 14, where the topology influences the results: the genus-1 part of the query is matched with the back of the chair (rank 6) while its left bent appendix is matched with one of the chair's (rank 6) and table's (rank 7) legs (the unfolding signatures are bending insensitive). In the future, the combination of local and structural approaches is worth being studied to overcome this issue.

6. Application to Modelling by Example

To demonstrate the applicative interest of the framework, we designed an intelligent modelling-by-example system [FKS*04]. Figures 20 and 21 show typical use examples. First, the user queries the data-set through our partial shape retrieval system. Then, he/she selects on the query the Reeb patterns (or Reeb pattern sub-parts) he/she wants to remove (in red, green and blue in figure 20(a)). Next, the system automatically highlights the parts of the retrieved results candidates for swapping, based on our graph matching algorithm. The user then selects the retrieved results and cut the desired parts (highlighted or not, figures 20(c), 20(d) and 20(f)). After scaling, rotating and translating the parts according to his/her needs, the cut sub-parts are pasted back onto the query model (figure 20(b)). In our experiments, boundaries are simply re-meshed but more visually appealing methods can be employed for gluing parts [SBSCO06]. Thanks to the partial shape retrieval and the part swapping suggestions, a novice user can intuitively and rapidly create new 3D shapes

(a) Query   (b) New model

(c) 1. s=0.22   (d) 2. s=0.20   (e) 3. s=0.19   (f) 4. s=0.18

Figure 20: *Modelling a cow-horse by example: the user selects on the query, then on the retrieved results (second row), the Reeb patterns to be exchanged.*

(a) Query   (b) New model

(c) 1. s=0.61   (d) 2. s=0.50   (e) 3. s=0.42   (f) 4. s=0.40

Figure 21: *Modelling a new woman model by example, composing both synthetic and scanned models.*

with high geometric details based on the example parts of interest retrieved by our system.

7. Conclusion

In this paper, we presented a novel approach for fast and efficient partial 3D shape retrieval. The main contribution of this work was to take advantage of Reeb graph theory properties to improve both the shape description and comparison processes. Extensive experiments demonstrated the improvement of each of these steps, resulting in an overall gain of, respectively, *14.1%* and *40.9%* on the methods by Biasotti *et al.* [BMSF06] and Cornea *et al.* [CDS*05]. Moreover, the robustness to rigid and non-rigid transformations and surface noise has been shown. Finally, queries are processed in interactive time (from 4 to 30 seconds).

However, shape topological description might be too discriminant in some particular cases. For example, humanoids can be modelled with closed fists or open hands, resulting in different Reeb graphs and thus penalized partial similarity. This is a major drawback of topology-based approaches. In the future, the combination of local and structural approaches is worth being studied.

Moreover, input surface models are required to be manifold. In the future, we would like to adapt the framework to more general mesh models. Reeb graph construction algorithms for non-manifold surfaces can be a starting point [PSBM07].

Finally, as dynamic meshes (3D plus time) are becoming more and more popular, in the future, we would like to investigate the use of Reeb graphs of higher dimension manifolds [EHMP04] for the partial retrieval of 3D dynamic shapes. We believe this research topic is one of the next challenges of the shape retrieval community and could result in nice user applications like *animation-by-example* systems.
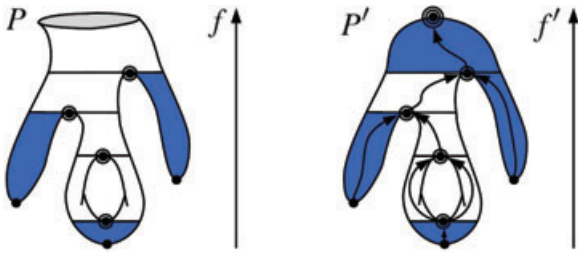
Appendix A: $n_D(P) = n_A(P) + 1 - 3g_P$

Proof Let f be a simple Morse function defined on a compact closed and orientable 2-manifold M and $R(f)$ its Reeb graph.

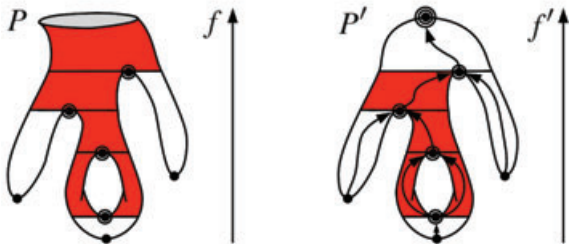Let P be a Reeb pattern defined relatively to $R(f)$. By definition, P is a compact 2-manifold with one boundary component.

Let P' be the compact and orientable 2-manifold without boundary obtained by the closure of the boundary of P (where the unique boundary component of P is glued by contraction to a point, as shown in Figures 22 and 23). Let f' be a simple Morse function defined on P' such that it has the

Figure 22: *Enumeration of the disk-like Reeb charts of a Reeb pattern. Left: Original Reeb pattern P. Right: Reeb pattern P′ after the closure of the unique boundary component of P. Disk-like Reeb charts are in blue.*

Annulus-like Reeb chart enumeration

Figure 23: *Enumeration of the annulus-like Reeb charts of a Reeb pattern. Left: Original Reeb pattern P. Right: Reeb pattern P′ after the closure of the unique boundary component of P. Annulus-like Reeb charts are in red.*

same set of critical points and critical values on P' than f on P, plus one maximum (due to the closure of the boundary component of P). f' has distinctly valued critical points and all its critical points are non-degenerate. f' is indeed a simple Morse function. For example, in Figures 22 and 23, f and f' are the height functions. Let $R(f')$ be the Reeb graph of f' (depicted by black arrows on Figures 22 and 23, right).

On the first hand, the Euler characteristic $\chi(P')$ of P' is given by the generalized Euler relation [FK97] (where $g_{P'}$ is the genus of P'):

$$\chi(P') = 2 - 2g_{P'}. \qquad (7)$$

On the other hand, the Euler characteristic $\chi(P')$ of P' can also be expressed by the Morse-Euler formula [FK97] since P' is a closed manifold (where $k = 2$ is the dimension of the manifold):

$$\chi(P') = \sum_{i=0}^{k}(-1)^i \mu_i(f') = \mu_0(f') - \mu_1(f') + \mu_2(f'). \qquad (8)$$

In Equation (8), $\mu_i(f')$ stands for the ith Morse number of f', which is equal to the number of f' critical points of index i. In particular, $\mu_0(f')$, $\mu_1(f')$ and $\mu_2(f')$ are, respectively, the

number of f' local minima, saddles and maxima. In Figures 22 and 23, each critical point is marked with a number of concentric circles equal to its index i.

Disk-like Reeb chart enumeration

Let $n_D(P')$ be the number of disk-like Reeb charts of P'. By definition, each disk-like Reeb chart of P' is exactly adjacent to one local extremum of f'. Moreover, the degree in $R(f')$ of equivalence classes of minima and maxima equals one [Ree46] (see Figure 22, right). Then, a local extremum of f' can only be adjacent to one disk-like Reeb chart of P'. Thus

$$n_D(P') = \mu_0(f') + \mu_2(f'). \qquad (9)$$

Moreover, by definition, f' has exactly the same set of critical points and critical values on P' than f on P, plus one maximum due to the closure of the boundary component of P (see Figure 22). Consequently, P and P' have the same Reeb chart decomposition at the exception of the chart adjacent to the additional maximum of f', which is transformed from an annulus-like Reeb chart (in P, Figure 22, left) to a disk-like Reeb chart (in P', Figure 22, right) by the closure of the unique boundary component of P. Hence

$$n_D(P) = n_D(P') - 1 = \mu_0(f') + \mu_2(f') - 1. \qquad (10)$$

Annulus-like Reeb chart enumeration

Let $n_A(P')$ be the number of annulus-like Reeb charts of P'. $R(f')$ is a finite and connected 1-D simplicial complex [Ree46]. Consequently, it can be considered as a planar graph, whose vertices are the equivalence classes corresponding to critical points of f' and whose edges correspond to the Reeb charts of P'. Then, the Euler relation for planar graphs holds

$$\chi(R(f')) = V_{R(f')} - E_{R(f')} + F_{R(f')} = 2, \qquad (11)$$

where $V_{R(f')}$ is the number of critical points of f':

$$V_{R(f')} = \mu_0(f') + \mu_1(f') + \mu_2(f'), \qquad (12)$$

where $E_{R(f')}$ is the number of Reeb charts of P':

$$E_{R(f')} = n_D(P') + n_A(P') \qquad (13)$$

and where $F_{R(f')}$ is the number of faces of the planar graph (with $L_{R(f')}$ the number of loops in $R(f')$):

$$F_{R(f')} = L_{R(f')} + 1. \qquad (14)$$

Moreover, $R(f')$ has $g_{P'}$ loops [CMEH*03] (with $g_{P'}$ the genus of P'). Then, Equations (11), (12), (13) and (14) become:

$$\chi(R(f')) = 2 = \mu_0(f') + \mu_1(f') + \mu_2(f')$$
$$- (n_D(P') + n_A(P')) + g_{P'} + 1. \qquad (15)$$

Thanks, to Equation (9), we have:

$$2 = \mu_1(f') - n_A(P') + g_{P'} + 1$$
$$n_A(P') = \mu_1(f') + g_{P'} - 1. \qquad (16)$$

Moreover, by definition, f' has exactly the same set of critical points and critical values on P' than f on P, plus one maximum due to the closure of the unique boundary component of P (see Figure 23). Consequently, P and P' have the same Reeb chart decomposition at the exception of the chart adjacent to the additional maximum of f', which is transformed from an annulus-like Reeb chart (in P, Figure 23, left) to a disk-like Reeb chart (in P', Figure 23, right) by the closure of the unique boundary component of P. Hence

$$n_A(P) = n_A(P') + 1$$
$$n_A(P) = \mu_1(f') + g_{P'}. \qquad (17)$$

Relation between $n_D(P)$ and $n_A(P)$

Consequently to Equations (10) and (17), Equation (8) becomes:

$$\chi(P') = \mu_0(f') - \mu_1(f') + \mu_2(f')$$
$$\chi(P') = n_D(P) + 1 - (n_A(P) - g_{P'}). \qquad (18)$$

Therefore, thanks to the Equation (7), we have the following relations:

$$n_D(P) + 1 - n_A(P) + g_{P'} = 2 - 2g_{P'}$$
$$n_D(P) = n_A(P) + 1 - 3g_{P'}. \qquad (19)$$

Moreover, by definition, the boundary of a Reeb pattern is required to be composed of a single connected component. Then, the boundary of a Reeb pattern cannot lie on a topological handle. Consequently, the closure of the unique boundary component of P cannot modify its genus g_P. Then

$$g_P = g_{P'}. \qquad (20)$$

Thanks to the Equation (20), we have the final result:

$$n_D(P) = n_A(P) + 1 - 3g_P. \qquad (21)$$

References

[AHLD07] AUJAY G., HÉTROY F., LAZARUS F., DEPRAZ C.: Harmonic skeletons for realistic character animation. In *Symposium on Computer Animation* (2007), pp. 151–160.

[BGSF08] BIASOTTI S., GIORGI D., SPAGNUOLO M., FALCIDIENO B.: Reeb graphs for shape analysis and applications. *Theoretical Computer Science 392* (2008), 5–22.

[BKS*05] BUSTOS B., KEIM D. A., SAUPE D., SCHRECK T., VRANIC D. V.: Feature-based similarity search in 3D object databases. *ACM Computing Surveys 37* (2005), 345–387.

[BMS00] BIASOTTI S., MORTARA M., SPAGNUOLO M.: Surface compression and reconstruction using Reeb graphs and shape analysis. In *Spring Conference on Computer Graphics* (2000), pp. 175–184.

[BMSF06] BIASOTTI S., MARINI S., SPAGNUOLO M., FALCIDIENO B.: Sub-part correspondence by structural descriptors of 3D shapes. *Computer-Aided Design Journal 38* (2006), 1002–1019.

[CDS*05] CORNEA N. D., DEMIRCI M. F., SILVER D., SHOKOUFANDEH A., DICKINSON S., KANTOR P. B.: 3D object retrieval using many-to-many matching of curve skeletons. In *IEEE Shape Modeling International* (2005), pp. 366–371.

[CMEH*03] COLE-MCLAUGHLIN K., EDELSBRUNNER H., HARER J., NATARAJAN V., PASCUCCI V.: Loops in Reeb graphs of 2-manifolds. In *Symposium on Computational Geometry* (2003), pp. 344–350.

[CSM03] COHEN-STEINER D., MORVAN J.-M.: Restricted delaunay triangulations and normal cycle. In *Symposium on Computational Geometry* (2003), pp. 312–321.

[CTSO03] CHEN D. Y., TIAN X. P., SHEN Y. T., OUHYOUNG M.: On visual similarity based 3D model retrieval. *Computer Graphics Forum 22* (2003), 223–232.

[DJ06] DEY T. K., JIAN S.: Defining and computing curve skeletons with medial geodesic function. In *Eurographics Symposium on Geometry Processing* (2006), pp. 143–152.

[EHMP04] EDELSBRUNNER H., HARER J., MASCARENHAS A., PASCUCCI V.: Time-varying Reeb graphs for continuous space-time data. In *Symposium on Computational Geometry* (2004), pp. 366–372.

[EHZ01] EDELSBRUNNER H., HARER J., ZOMORODIAN A.: Hierarchical Morse-Smale complexes for piecewise linear 2-manifolds. In *Symposium on Computational Geometry* (2001), pp. 70–79.

[FK97] FOMENKO A., KUNII T.: *Topological Modeling for Visualization*. Springer-Verlag, 1997.

[FKS*04] FUNKHOUSER T., KAZHDAN M., SHILANE P., MIN P., KIEFER W., TAL A., RUSINKIEWICZ S., DOBKIN D.: Modeling by example. *ACM Transactions on Graphics 23* (2004), 652–663.

[FMK*03] FUNKHOUSER T., MIN P., KAZHDAN M., CHEN J., HALDERMAN A., DOBKIN D.: A search engine for 3D models. *ACM Transactions on Graphics 22* (2003), 83–105.

[FS06]   FUNKHOUSER T., SHILANE P.: Partial matching of 3D shapes with priority-driven search. In *Eurographics Symposium on Geometry Processing* (2006), pp. 131–142.

[GCO06]   GAL R., CCOHEN-OR D.: Salient geometric features for partial shape matching and similarity. *ACM Transactions on Graphics 25* (2006), 130–150.

[GSCO07]   GAL R., SHAMIR A., COHEN-OR D.: Pose oblivious shape signature. *IEEE Transactions on Visualization and Computer Graphics 13* (2007), 261–271.

[HKDH04]   HUBER D., KAPURIA A., DONAMUKKALA R., HEBERT M.: Parts-based 3D object classification. In *IEEE Computer Vision and Pattern Recognition* (2004), pp. 82–89.

[HSKK01]   HILAGA M., SHINAGAWA Y., KOHMURA T., KUNII T.: Topology matching for fully automatic similarity estimation of 3D shapes. In *SIGGRAPH* (2001), pp. 203–212.

[IJL*05]   IYER N., JAYANU S., LOU K., KALYANARAMAN Y., RAMANI K.: Three-dimensional shape searching: State-of-the-art review and future trends. *Computer-Aided Design Journal 37* (2005), 509–530.

[JH99]   JOHNSON A. E., HEBERT M.: Using spin-images for efficient multiple model recognition in cluttered 3D scenes. *IEEE Transactions on Pattern Analysis and Machine Intelligence 21* (1999), 433–449.

[JZ07]   JAIN V., ZHANG H.: A spectral approach to shape-based retrieval of articulated 3D models. *Computer-Aided Design Journal 39* (2007), 398–407.

[KLT05]   KATZ S., LEIFMAN G., TAL A.: Mesh segmentation using feature point and core extraction. *The Visual Computer 21* (2005), 865–875.

[KSDD03]   KESELMAN Y., SHOKOUFANDEH A., DEMIRCI M., DICKINSO S.: Many-to-many graph matching via metric embedding. In *IEEE Computer Vision and Pattern Recognition* (2003), pp. 850–857.

[LZ07]   LIU R., ZHANG H.: Mesh segmentation via spectral embedding and contour analysis. *Computer Graphics Forum 26* (2007), 385–394.

[LZQ06]   LIU Y., ZHA H., QIN H.: Shape topics: a compact representation and new algorithms for 3D partial shape retrieval. In *IEEE Computer Vision and Pattern Recognition* (2006), pp. 2025–2032.

[MB98]   MESSMER B. T., BUNKE H.: A new algorithm for error-tolerant subgraph isomorphism detection. *IEEE Transactions on Pattern Analysis and Machine Intelligence 20* (1998), 493–504.

[MGP06]   MITRA N. J., GUIBAS L., PAULY M.: Partial and approximate symmetry detection for 3D geometry. *ACM Transactions on Graphics 25* (2006), 560–568.

[Mil63]   MILNOR J.: *Morse Theory*. Princeton University Press, 1963.

[MPB07]   MARINI S., PARABOSCHI L., BIASOTTI S.: SHape Retrieval Contest 2007: Partial matching track. In *SHREC (in conjunction with IEEE Shape Modeling International)* (2007), pp. 13–16.

[NGH04]   NI X., GARLAND M., HART J.: Fair Morse functions for extracting the topological structure of a surface mesh. *ACM Transactions on Graphics 23* (2004), 613–622.

[PSBM07]   PASCUCCI V., SCORZELLI G., BREMER P. T., MASCARENHAS A.: Robust on-line computation of Reeb graphs: Simplicity and speed. *ACM Transactions on Graphics 26* (2007), 58.1–58.9.

[Ree46]   REEB G.: Sur les points singuliers d'une forme de Pfaff complètement intégrable ou d'une fonction numérique. *Comptes-rendus des Séances de l'Académie des Sciences 222* (1946), 847–849.

[SBSCO06]   SHARF A., BLUMENKRANTS M., SHAMIR A., COHEN-OR D.: Snappaste: An interactive technique for easy mesh composition. *The Visual Computer 22* (2006), 835–844.

[TS05]   TUNG T., SCHMITT F.: The augmented multiresolution Reeb graph approach for content-based retrieval of 3D shapes. *International Journal of Shape Modeling 11* (2005), 91–120.

[TV04]   TANGELDER J. W. H., VELTKAMP R. C.: A survey of content based 3D shape retrieval methods. In *IEEE Shape Modeling International* (2004), pp. 145–156.

[TVD07]   TIERNY J., VANDEBORRE J.-P., DAOUDI M.: Reeb chart unfolding based 3D shape signatures. In *Eurographics* (2007), pp. 13–16.

[TVD08]   TIERNY J., VANDEBORRE J.-P., DAOUDI M.: Enhancing 3D mesh topological skeletons with discrete contour constrictions. *The Visual Computer 24* (2008), 155–172.

[WWJ06]   WANG S., WANG Y., JIN M., GG X., SAMARAS D.: 3D surface matching and recognition using conformal geometry. In *IEEE Computer Vision and Pattern Recognition* (2006), pp. 2453–2460.

[ZMT05]   ZHANG E., MISCHAIKOW K., TURK G.: Feature-based surface parametrization and texture mapping. *ACM Transactions on Graphics 24* (2005), 1–27.